Title: Sharyginite, Ca3TiFe2O8, A New Mineral from the Bellerberg Volcano, Germany

Author: Rafał Juroszek , Hannes Krüger, Irina Galuskina, Biljana Krüger, Lidia Jeżak, Bernd Ternes, Tomasz Krzykawski, Evgeny Galuskin i in.

Citation style: Juroszek Rafał, Krüger Hannes, Galuskina Irina, Krüger Biljana, Jeżak Lidia, Ternes Bernd, Krzykawski Tomasz, Galuskin Evgeny i in. (2018). Sharyginite, Ca3TiFe2O8, A New Mineral from the Bellerberg Volcano, Germany. "Minerals" (Vol. 8, iss. 7 (2018), Art. No. 308), doi 10.3390/min8070308

UNIWERSYTET ŚLĄSKI W KATOWICACH — Biblioteka Uniwersytetu Śląskiego — Ministerstwo Nauki i Szkolnictwa Wyższego

minerals

MDPI

Sharyginite, Ca$_3$TiFe$_2$O$_8$, A New Mineral from the Bellerberg Volcano, Germany

Rafał Juroszek [1,*] **, Hannes Krüger** [2] **, Irina Galuskina** [1] **, Biljana Krüger** [2] **, Lidia Jeżak** [3] **, Bernd Ternes** [4] **, Justyna Wojdyla** [5] **, Tomasz Krzykawski** [1] **, Leonid Pautov** [6] **and Evgeny Galuskin** [1]

[1] Department of Geochemistry, Mineralogy and Petrography, Faculty of Earth Sciences, University of Silesia, Będzińska 60, 41-200 Sosnowiec, Poland; irina.galuskina@us.edu.pl (I.G.); tomasz.krzykawski@us.edu.pl (T.K.); evgeny.galuskin@us.edu.pl (E.G.)

[2] Institute of Mineralogy and Petrography, University of Innsbruck, Innrain 52, 6020 Innsbruck, Austria; Hannes.Krueger@uibk.ac.at (H.K.); Biljana.Krueger@uibk.ac.at (B.K.)

[3] Institute of Geochemistry, Mineralogy and Petrology, University of Warsaw, Al. Żwirki and Wigury 93, 02-089 Warszawa, Poland; l.jezak@uw.edu.pl

[4] Dienstleistungszentrum Ländlicher Raum (DLR) Westerwald-Osteifel-Aussenstelle Mayen, Bahnhofstrasse 45, DE-56727 Mayen, Germany; Bernd.Ternes@dlr.rlp.de

[5] Swiss Light Source, Paul Scherrer Institute, 5232 Villigen, Switzerland; justyna.wojdyla@psi.ch

[6] Fersman Mineralogical Museum RAS, Leninskiy pr, 18/2, 115162 Moscow, Russia; pla58@mail.ru

* Correspondence: rjuroszek@us.edu.pl; Tel.: +48-516-491-438

check for updates

Abstract: The new mineral sharyginite, Ca$_3$TiFe$_2$O$_8$ ($P2_1ma$, Z = 2, a = 5.423(2) Å, b = 11.150(8) Å, c = 5.528(2) Å, V = 334.3(3) Å^3), a member of the anion deficient perovskite group, was discovered in metacarbonate xenoliths in alkali basalt from the Caspar quarry, Bellerberg volcano, Eifel, Germany. In the holotype specimen, sharyginite is widespread in the contact zone of xenolith with alkali basalt. Sharyginite is associated with fluorellestadite, cuspidine, brownmillerite, rondorfite, larnite and minerals of the chlormayenite-wadalite series. The mineral usually forms flat crystals up to 100 μm in length, which are formed by pinacoids {100}, {010} and {001}. Crystals are flattened on (010). Sharyginite is dark brown, opaque with a brown streak and has a sub-metallic lustre. In reflected light, it is light grey and exhibits rare yellowish-brown internal reflections. The calculated density of sharyginite is 3.943 g·cm^{-3}. The empirical formula calculated on the basis of 8 O *apfu* is Ca$_{3.00}$(Fe$^{3+}_{1.00}$Ti$^{4+}_{0.86}$Mn$^{4+}_{0.11}$Zr$_{0.01}$Cr$^{3+}_{0.01}$Mg$_{0.01}$)$_{\Sigma 2}$(Fe$^{3+}_{0.76}$Al$_{0.20}$Si$_{0.04}$)$_{\Sigma 1.00}$O$_8$. The crystal structure of sharyginite, closely related to shulamitite Ca$_3$TiFeAlO$_8$ structure, consists of double layers of corner-sharing (Ti, Fe^{3+}) O$_6$ octahedra, which are separated by single layers of (Fe^{3+}O$_4$) tetrahedra. We suggest that sharyginite formed after perovskite at high-temperature conditions >1000°C.

Keywords: sharyginite; new mineral; crystal structure; Raman spectroscopy; Bellerberg volcano; Germany

1. Introduction

Sharyginite, Ca$_3$TiFe$_2$O$_8$, is a new mineral which was found in thermally-metamorphosed limestone xenoliths in alkali basalts of the Bellerberg volcano lava field, Caspar quarry, Eastern Eifel region, Rhineland-Palatinate, Germany (50°21′6″ N, 7°14′2″ E). Sharyginite ($P2_1ma$, Z = 2, a = 5.423(2) Å, b = 11.150(8) Å, c = 5.528(2) Å, V = 334.3(3) Å^3) is a Fe^{3+}-analogue of shulamitite, Ca$_3$TiFeAlO$_8$ [1], a member of the anion deficient perovskite group [2] and also an intermediate member of the pseudobinary perovskite CaTiO$_3$—brownmillerite Ca$_2$(Fe,Al)$_2$O$_5$ series [3].

"Grenier phase" is the name of the Ca$_3$TiFe$^{3+}_2$O$_8$ compound synthesized in 1976 [4]. This phase was intensively studied due to its ionic and electronic conductivity [4,5]. The crystal structure of

$Ca_3TiFe^{3+}{}_2O_8$ was first determined by Rodriguez-Carvajal and co-authors [6]. Some information on magnetic properties of this phase were reported by Causa et al. as result of an electron paramagnetic resonance (EPR) study [7].

Previously, sharyginite was documented as a mineral in ye'elimite-larnite pyrometamorphic rocks of the Hatrurim Complex [3] and in high-temperature skarns occurring in sedimentary carbonate xenoliths within ignimbrite confined to the Upper Chegem volcanic structure of the North Caucasus, Kabardino-Balkaria, Russia [8]. Some sharyginite crystals were recognized in mineral association of Ca-rich xenoliths in Klöch Basalt quarry, Bad Radkersburg, Styria, Austria [9]. This phase was also described in metacarbonate rocks from some burned dumps of the Donetsk [10] and Chelyabinsk [11] coal basins. Moreover, it was identified in xenoliths from the Eifel region [12], but because of the small size of the crystals, this mineral was not studied in detail, until now.

Sharyginite (IMA 2017-14) was approved by the Commission of New Minerals, Nomenclature and Classification of IMA. Type material was deposited in the mineralogical collection of Fersman Mineralogical Museum RAS, Leninskiy pr., 18/2, 115162 Moscow, Russia, catalogue numbers: 4958/1.

The name sharyginite was given in honour of Victor Victorovich Sharygin (b.1964) from the Sobolev Institute of Geology and Mineralogy, Novosibirsk, Russia. Victor Sharygin is a mineralogist, author and co-author of many publications concerning the mineralogy and petrology of different alkaline rocks (alkali basalts, lamproites, kimberlites, carbonatites, etc.) and pyrometamorphic rocks. He is the author of new mineral descriptions; for example, shulamitite $Ca_3TiFeAlO_8$—Al-analogue of sharyginite [1]. He has also worked on xenolith specimens with sharyginite from Eifel and published some preliminary data on this mineral [12].

In the present paper, we report the detailed description of the new mineral sharyginite from the type locality—Caspar quarry, Bellerberg volcano, Eifel, Germany. In addition, we discuss the composition and Raman spectroscopic data of sharyginite from the other two localities: Upper Chegem volcanic Caldera, Great Caucasus, Russia and Jabel Harmun (Hatrurim Complex), Palestinian Autonomy.

2. Occurrence, Geological Settings, Physical and Optical Properties of Sharyginite

The type locality of sharyginite, is a part of a quaternary volcano region in the Eastern Eifel area, Rhineland-Palatinate, Germany [13]. The Bellerberg volcano is a well-preserved cinder cone: the western part of the crater wall is the actual Ettringer Bellerberg and the eastern one is the Kottenheimer Büden [14]. More than 20 new mineral species were discovered in the area of the Bellerberg volcano [13,15–17]. The active quarry is characterized by the presence of various thermally-metamorphosed silicate and carbonate-silicate xenoliths within a leucite tephrite lava [13,14]. The significant variety of xenoliths is based on different protolith composition and metamorphic transformations. The calcium-rich xenoliths in the crater area of the Bellerberg are mainly composed of gehlenite, pyroxene (diopside), garnet (grossular-andradite), anorthite, and wollastonite. As accessory minerals, chalcopyrite, hematite, magnetite, or spinel are noted. Some of these xenoliths contain larnite, jasmundite, brownmillerite, mayenite, spurrite, and monticellite. The appearance of such mineral assemblages is a result of metamorphism at very high-temperature conditions (pyrometamorphism). The altered limestone xenoliths are known for their diversity of secondary, low-temperature minerals. Ettringite is the most abundant. Portlandite, thaumasite, hydrocalumite, afwillite, tobermorite, $CaCO_3$ polymorphs, and zeolites belong to the low-temperature mineral association [14].

The new mineral sharyginite occurs in altered Ca-rich xenolith, which consists of a few multi-coloured zones characterized by variable mineral associations (Figure 1). The first zone (light brown and pink) is composed of cuspidine, andradite, and minerals of the brownmillerite-srebrodolskite series. Lakargiite, sphalerite, and some Ni-phosphides occur as accessory minerals. Secondary phases are represented by hydrocalumite, ettringite, calcite, brucite, hydrogarnets, and unidentified Ca-hydrosilicates. The second zone (white and creamy) consists of cuspidine and minerals of the brownmillerite-srebrodolskite and chlormayenite-wadalite series.

Rankinite, fluorellestadite, vorlanite, lakargiite, and bismoclite appear in this zone as accessory minerals. The low-temperature mineral association is the same as in the first zone.
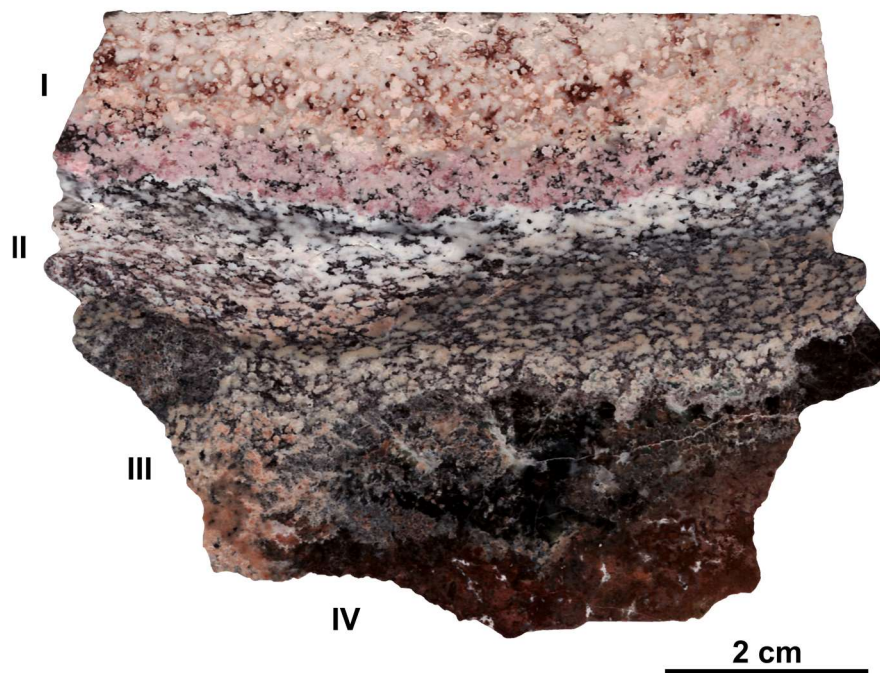

Figure 1. Xenolith specimen from Bellerberg with characteristic multi-coloured zones: I-III—xenolith, IV—altered alkali basalt (description in text).

Sharyginite is common in the next zone (Figure 1, zone III). It is associated with fluorellestadite, cuspidine, brownmillerite, rondorfite, larnite, and minerals of the chlormayenite-wadalite series (Figure 2a). Rankinite, magnesioferrite, perovskite, and fluorite are less common in this zone. Low-temperature mineral assemblages are represented by calcite, ettringite-thaumasite, brucite, gypsum and Ca-hydrosillicates. Sharyginite forms euhedral crystals and their intergrowths, which can be up to 200 μm in size (Figure 2b). Abundant inclusions of cuspidine, fluorellestadite, and also chlormayenite are characteristic for sharyginite crystals (Figure 2c). The next zone is represented by completely altered basalt (Figure 1, zone IV). This zone, about 2 cm thick, consists of cuspidine, perovskite, minerals of the chlormayenite-wadalite series, and magnesioferrite. Sharyginite is also noted. In some cavities, clinoenstatite and spinel relicts occur. The low-temperature association is represented by calcite, gypsum, gibbsite, and minerals of ettringite-thaumasite series.

Sharyginite crystals are formed by pinacoids {100}, {010}, {001}, and the rhombic pyramid is observed rarely. Crystals are flattened on (010) (Figure 3). Sharyginite exhibits a dark brown colour and a brown streak. The mineral is opaque in transmitted light and exhibits a sub-metallic lustre. Sharyginite shows good cleavage on (010) and imperfect along (001) and (100). Parting was not observed, tenacity is brittle and fracture is uneven.
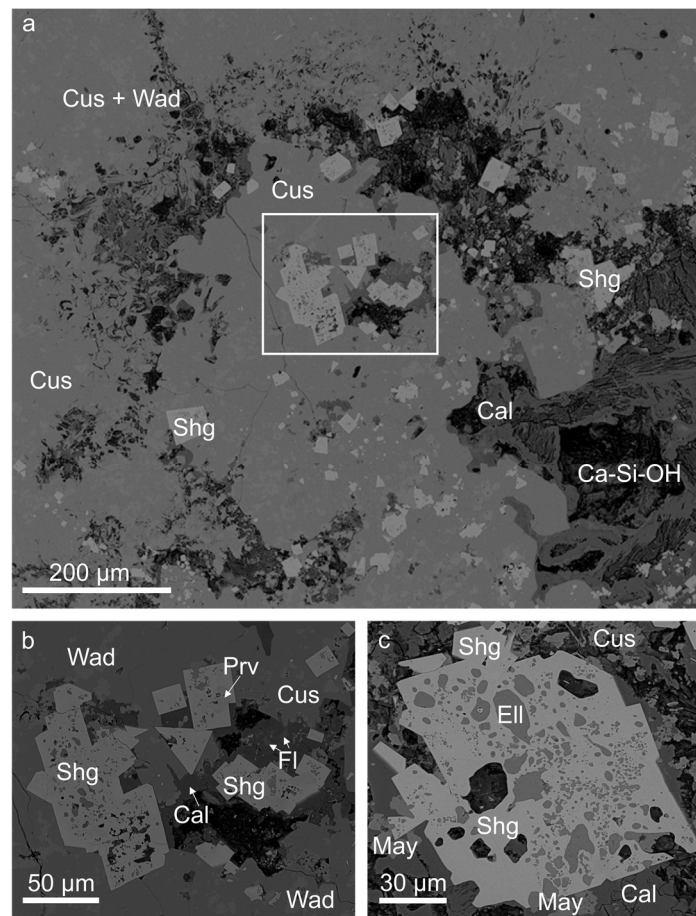
Figure 2. (**a**) General view of a metacarbonate xenolith with sharyginite from the Caspar quarry, Bellerberg volcano; fragment in the frame is magnified in Figure 2b; (**b**) Euhedral crystals and intergrowths of sharyginite; (**c**) Poikilitic crystal of sharyginite with inclusions of fluorellestadite and chlormayenite. BSE (backscattered electron) images. Cal—calcite; Ca-Si-OH—Ca-hydrosilicates; Cus—cuspidine; Ell—fluorellestadite; Fl—fluorite; May—chlormayenite; Prv—perovskite; Shg—sharyginite; Wad—wadalite.
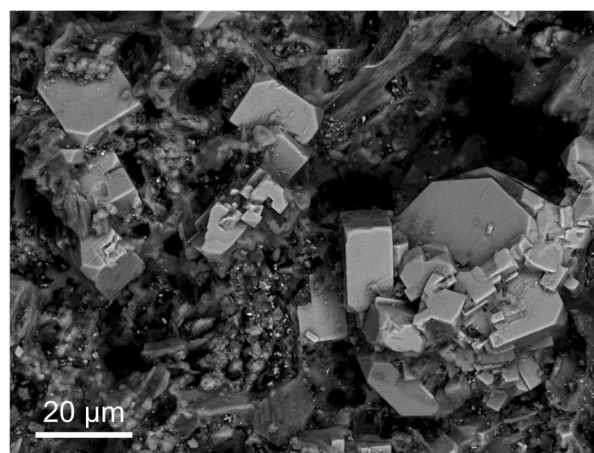
Figure 3. Sharyginite crystals formed by pinacoids {100}, {010}, and {001}, and rhombic pyramid and flattened on (010) at the part of the strongly altered rock. BSE image.

The density could not be measured because of abundant fluorellestadite, chlormayenite, and cuspidine inclusions. The density calculated using the average composition and unit-cell parameters as obtained from single crystal XRD (X-ray Powder Diffraction) analysis is 3.943 g·cm^{-3}. Micro-hardness measurements were carried out using a VHN (Vickers Hardness Number) load of 25 g which gave a mean value of 635 kg/mm^3 (range from 621 to 649 kg/mm^3) based on 35 measurements. This value corresponds to a hardness of ~5.5–6 in the Mohs scale.

In reflected light, sharyginite was characterized by light grey colour and weak pleochroism from grey to very light grey. Under crossed polarizers, weak anisotropy was noted. Rare yellowish brown internal reflections were observed in sharyginite crystals in polarized light (Figure 4).
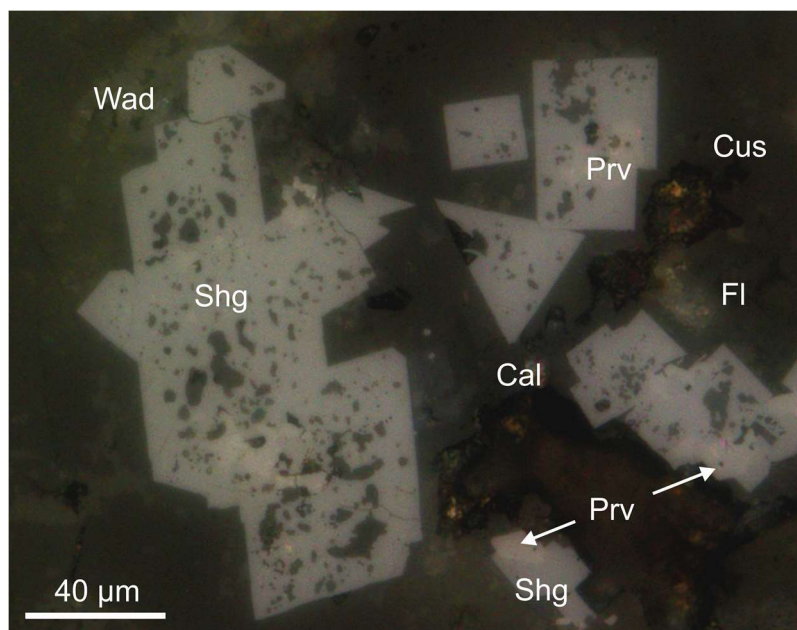
Figure 4. Sharyginite crystals with characteristic yellowish brown internal reflections from the Bellerberg volcano. Reflected light, crossed polarizers. Cal—calcite; Cus—cuspidine; Fl—fluorite; Prv—perovskite; Shg—sharyginite; Wad—wadalite.

Quantitative reflectance measurements for sharyginite from the Bellerberg volcano were measured in air relative to a SiC standard using a UMSP 50D Opton microscope-spectrophotometer (Table 1). Reflectance percentages for the four R_{max} and R_{min} COM (Commission on Ore Mineralogy) wavelengths were: 16.1, 15.5 (470 nm); 14.9, 14.2 (546 nm); 14.6, 14.1 (589 nm), and 14.5, 13.9 (650 nm).

Table 1. Reflectance values for sharyginite.

R_{max}/R_{min} (%)	λ (nm)	R_{max}/R_{min} (%)	λ (nm)
18.7/17.6	400	14.8/14.2	560
18.3/17.4	420	14.7/14.1	580
17.0/16.0	440	14.6/14.1	589 (COM)
16.4/15.6	460	14.6/14.1	600
16.1/15.5	470 (COM)	14.6/14.0	620
15.9/15.4	480	14.6/14.0	640
15.5/14.9	500	14.5/13.9	650 (COM)
15.2/14.5	520	14.4/13.7	660
15.0/14.3	540	14.3/13.5	680
14.9/14.2	546 (COM)	14.1/13.4	700

Sharyginite was also detected in other localities. It was found in the xenolith No.1—the largest of the 11 described altered carbonate xenoliths within ignimbrites of the Upper Chegem volcanic Caldera, North Caucasus, Kabardino-Balkaria, Russia. This unique xenolith was discovered by Victor Gazeev and Alexandr Zadov [18] and specified as a pyrometamorphic rock, formed at high temperature and low-pressure conditions [19]. The Upper Chegem Caldera situated in the eastern part of the Elbrus-Kyugen volcanic region is a type locality for more than 20 new mineral species e.g.: lakargiite, $CaZrO_3$ [8], chegemite, $Ca_7(SiO_4)_3(OH)_2$ [20], elbrusite, $Ca_3(Zr_{1.5}U^{6+}_{0.5})Fe^{3+}_3O_{12}$ [21], rusinovite, $Ca_{10}(Si_2O_7)_3Cl_2$ [22], pavlovskyite, $Ca_8(SiO_4)_2(Si_3O_{10})$ [23], edgrewite, $Ca_9(SiO_4)_4F_2$ [24], dzhuluite, $Ca_3SbSnFe^{3+}_3O_{12}$ [25], etc. More geological information concerning this locality can be found in Gazeev et al. [18], Galuskin et al. [8,20] and Galuskina et al. [26].

In the analysed specimen, sharyginite occurs as an accessory mineral. Cuspidine, fluorellestadite, wadalite, and larnite are widespread rock-forming minerals. Less commonly sharyginite is associated with perovskite, lakargiite, periclase, fluorite, and baryte. Secondary minerals are represented by low-temperature phases belonging to the ettringite-thaumasite series and unidentified Ca-hydrosilicates. Sharyginite from this locality occurs as euhedral and subhedral crystals up to 200 μm in size (Figure 5a). Most of them are partially or totally altered and replaced by phases exhibiting compositions similar to iron oxides. Unaltered sharyginite up to 50 μm in size was observed rarely as single crystals in a matrix of ellestadite-wadalite. Mostly, they are characterized by the presence of wadalite inclusions (Figure 5b).
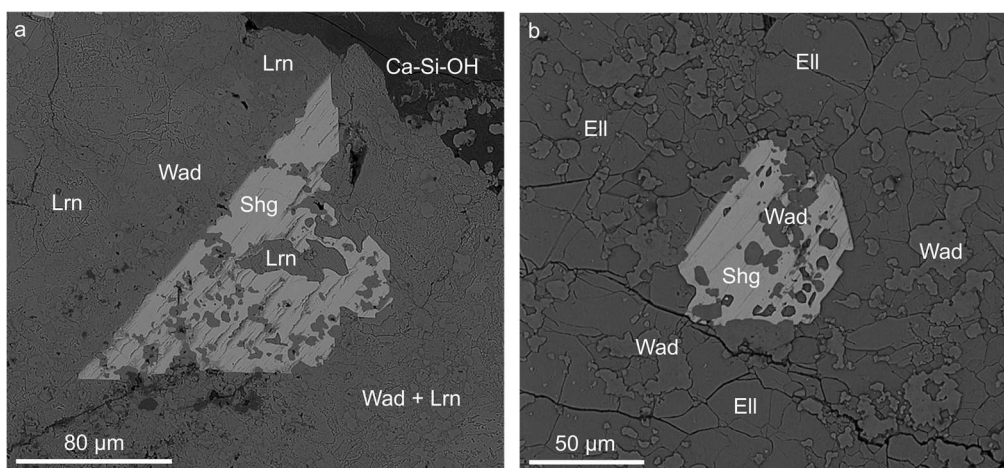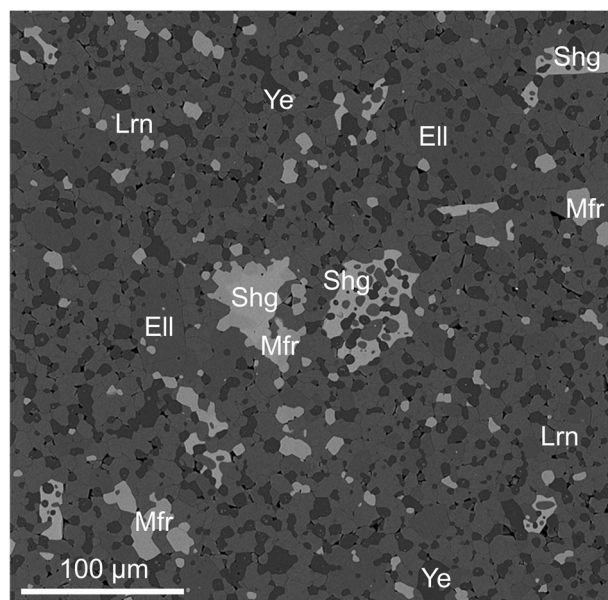

Figure 5. (**a**) Sharyginite crystal in larnite-wadalite rock from the Upper Chegem volcanic Caldera; (**b**) Poikilitic euhedral crystal of sharyginite with wadalite inclusions. BSE images. Ca-Si-OH—Ca-hydrosilicates, Ell—fluorellestadite, Lrn—larnite, Shg—sharyginite, Wad—wadalite.

Sharyginite was also found in larnite-ye'elimite nodules from pseudoconglomerates of the pyrometamorphic rocks of the Hatrurim Complex, Jabel Harmun locality, Judean Mountains, Palestinian Autonomy. Jabel Harmun, as well as other Hatrurim Complex localities, consists of high-temperature rocks represented, mainly, by larnite-, gehlenite- and spurrite-bearing rocks [27]. It is also the type locality for a few new minerals such as: vapnikite, Ca_3UO_6 [27], harmunite, $CaFe_2O_4$ [28], fluormayenite, $Ca_{12}Al_{14}O_{32}F_2$ [29], nabimusaite, $KCa_{12}(SiO_4)_4(SO_4)_2O_2F$ [30], gazeevite, $BaCa_6(SiO_4)_2(SO_4)_2O$ [31] and dzierżanowskite, $CaCu_2S_2$ [32]. Larnite-bearing rocks, which were formed during spontaneous combustion metamorphism of bituminous chalks and marls from the Ghareb and Taqiye Formations [33–36], were collected during fieldworks in 2015. Detailed geological description of the Jabel Harmun locality and the main hypotheses of the Hatrurim Complex formation were described by Galuskina et al. [28].

Sharyginite from Jabel Harmun was recognized in dark-brown homogenous larnite-ye'elimite rock samples, wherein magnesioferrite and minerals of the fluorellestadite-fluorapatite series occurred

also as main phases. Accessory and secondary minerals are represented by vorlanite, cuprite, tenorite, baryte, and hydrocalumite. Most frequently, sharyginite forms xenomorphic crystals from20 to 140 μm in size. Poikilitic crystals of sharyginite contain numerous inclusions of larnite, ye'elimite, and fluorellestadite. Homogenous grains occur rarely. Aggregates of sharyginite-magnesioferrite intergrowths up to 70 μm in size were more often noted (Figure 6).

Figure 6. Xenomorphic sharyginite crystals in larnite-ye'elimite rock from Jabel Harmun. BSE image. Ell—fluorellestadite, Lrn—larnite, Mfr—magnesioferrite; Shg—sharyginite, Ye—ye'elimite.

3. Materials and Methods

Mineral association and crystal morphology of sharyginite were examined using a scanning electron microscope Phenom XL, PhenomWorld, ThermoFisher Scientific, Eindhoven, The Netherlands equipped with an EDS (energy-dispersive X-ray spectroscopy) detector (Faculty of Earth Sciences, University of Silesia, Sosnowiec, Poland).

Quantitative chemical analyses of sharyginite were carried out using a CAMECA SX100 electron-microprobe operating in WDS (wavelength dispersive X-ray spectroscopy) mode (Institute of Geochemistry, Mineralogy and Petrology, University of Warsaw, Warsaw, Poland) at 15 kV and 10 nA, beam size ~1 μm. The following lines and standards were used: Ca$K\alpha$, Si$K\alpha$, Mg$K\alpha$—diopside; Al$K\alpha$—orthoclase; Ti$K\alpha$—rutile; Cr$K\beta$—Cr_2O_3; Fe$K\alpha$—Fe_2O_3; Sn$L\alpha$—cassiterite, Sr$L\alpha$—celestine; Mn$K\alpha$—rhodonite; Nb$L\alpha$—Nb; Zr$L\alpha$—zircon.

Powder X-ray diffraction data were obtained using Cu$K\alpha$ radiation (λ = 1.541874 Å) with 40 kV and 40 mA generator settings, on a Panalytical, X'Pert PRO PW3040/60 diffractometer equipped with an X'Celerator strip detector with an active angle of 2.122 °2θ, Malvern PANalytical, Almelo, Netherlands (Faculty of Earth Sciences, University of Silesia, Sosnowiec, Poland). Incident beam optics with divergence slit (1/8°) and anti-scatter slit (1/4°) was used. A Ni filter was used for reduction of the $K\beta$ line intensity. Conditions for recording the XRD pattern were as follow: scan range 5–90 °2θ, step size 0.01 °2θ, the counting time was set to 800 s. The total measurement time was 18 h.

Synchrotron radiation diffraction experiments were carried out at the Swiss Light Source (Paul Scherrer Institute, Villigen, Switzerland) beamline X06DA. The measurement was performed at ambient conditions and the data was collected with the Pilatus 2M-F detector placed at a distance of 120 mm from the crystal. The detector was vertically translated by 67 mm to increase the maximum resolution to 0.67 Å. The X-ray diffraction data were collected from a single crystal mounted onto the multi-axis PRIGo goniometer [37] using the DA+ acquisition software [38]. Data were collected at the

0.7085 Å wavelength with 0.1 s exposure time and 0.1° oscillation range using a focused 80×45 μm (h × v) beam. Data reduction, including empirical absorption correction, was performed with the XDS software package [39]. Further details of the intensity data collection and crystal-structure refinement of sharyginite are reported in Table 2.

Table 2. Parameters for X-ray data collection and crystal-structure refinement for sharyginite.

Crystal Data	
Chemical formula	$Ca_3TiFe_{1.68}Al_{0.32}O_8$
Crystal system	orthorhombic
Space group	$P2_1ma$
Unit-cell dimensions	$a = 5.423(2)$ Å
	$b = 11.150(8)$ Å
	$c = 5.528(2)$ Å
Unit cell volume	334.3(3) Å^3
Formula weight	398.6
Density (calculated)	3.943 g/cm^3
Z	2
Crystal size	$60 \times 40 \times 40$ μm
Data Collection	
Diffractometer	beamline X06DA, Swiss Light Source multi-axis goniometer PRIGo, PILATUS 2M-F detector
Radiation wavelength	0.7085 Å
Detector to sample distance	120 mm
Oscillation range	0.1°
No. of frames measured	1800
Time of exposure	0.1 s
Reflection ranges	$-7 \le h \le 7$; $-16 \le k \le 10$; $-7 \le l \le 7$
Reflection measured	1810
R_{int}	0.026
Refinement of Structure	**Full Matrix Least-squares on f**
No. of unique reflections	951
No. of observed unique refl. [$I > 3\sigma(I)$]	943
Final R values [$I > 3\sigma(I)$]	$R = 0.024$; $wR = 0.034$
Final R values (all data)	$R = 0.024$; $wR = 0.034$
S (all data)	1.62
Refined parameters	74
Weighting scheme	$w = 1/(\sigma^2(F) + 0.0001F^2)$
$\Delta\rho_{min}$ [e Å^{-3}]	-0.62
$\Delta\rho_{max}$ [e Å^{-3}]	0.49

The Raman spectra of sharyginite from Bellerberg, Jabel Harmun and Upper Chegem Caldera were recorded on a WITec alpha 300R Confocal Raman Microscope, WITec, Ulm, Germany (Faculty of Earth Science, University of Silesia, Poland) equipped with an air-cooled solid laser 532 nm and a CCD (closed circuit display) camera operating at $-61°C$. The laser radiation was coupled to a microscope through a single-mode optical fibre with a diameter of 3.5 μm. An air Zeiss (LD EC Epiplan-Neofluan DIC–100/0.75NA) objective was used. Raman scattered light was focused by effective Pinhole size about 30 μm and monochromator with a 600 mm^{-1} grating. The power of the laser at the sample position was 20–30 mW. Integration times of 5 s with an accumulation of 15 scans and a resolution of 3 cm^{-1} were chosen. The monochromator was calibrated using the Raman scattering line of a silicon plate (520.7 cm^{-1}). Spectra processing such as baseline correction and smoothing was performed using the Spectracalc software package GRAMS (Galactic Industries Corporation, NH, USA). Bands fitting

were done using a Gauss-Lorentz cross-product function, with the minimum number of component bands used for the fitting process.

4. Results

4.1. Chemical Composition

The analytical data for sharyginite from the Bellerberg volcano lava field (holotype locality), Jabel Harmun (Hatrurim Complex, Palestinian Autonomy) and Upper Chegem Volcanic Caldera (Kabardino-Balkaria, Russia) are presented in Table 3. Chemical data of other authors [1,3,12,40] are included in Table 4.

Table 3. The representative chemical composition of sharyginite from different localities.

wt %	Bellerberg (Holotype Locality)			Jabel Harmun (Hatrurim Complex)			Upper Chegem Caldera		
	Mean	S.D.	Range	Mean	S.D.	Range	Mean	S.D.	Range
	n = 9			n = 19			n = 4		
Nb_2O_5	n.d.			n.d.			n.d.		
MnO_2	2.27	0.71	1.04–3.22	n.d.			n.d.		
SiO_2	0.58	0.13	0.40–0.80	1.19	0.09	1.07–1.43	0.17	0.11	0.07–0.32
SnO_2	n.d.			n.d.			0.37	0.26	0.15–0.61
TiO_2	17.04	0.89	16.29–19.34	17.97	0.61	16.65–18.76	17.38	0.38	16.97–17.76
ZrO_2	0.27	0.14	0.07–0.57	0.43	0.11	0.25–0.62	0.39	0.23	0.16–0.67
Al_2O_3	2.49	0.53	2.22–3.89	3.83	0.14	3.62–4.13	1.86	0.45	1.36–2.29
Cr_2O_3	0.20	0.11	0.07–0.42	0.25	0.14	0.00–0.47	n.d.		
Fe_2O_3	34.87	0.85	32.81–35.85	32.80	0.79	31.70–34.54	37.43	1.03	36.40–38.72
CaO	41.59	0.37	40.99–42.09	42.19	0.27	41.64–42.60	40.71	0.14	40.53–40.85
FeO	n.d.			n.d.			n.d.		
MgO	0.13	0.05	0.08–0.24	0.08	0.02	0.06–0.11	0.05	0.01	0.04–0.06
MnO	n.d.			n.d.			0.09	0.06	0.01–0.13
SrO	n.d.			0.18	0.05	0.08–0.32	n.d.		
Total	99.44			98.91			98.45		

Table 3. *Cont.*

	Bellerberg (Holotype Locality)	Jabel Harmun (Hatrurim Complex)	Upper Chegem Caldera
		Calculated on 8 O	
Ca^{2+}	3.00	3.03	3.00
Sr^{2+}		0.01	0.00
Sum A	3.00	3.04	3.00
Nb^{5+}			
Mn^{4+}	0.11		
Sn^{4+}			0.01
Ti^{4+}	0.86	0.91	0.90
Zr^{4+}	0.01	0.01	0.01
Cr^{3+}	0.01	0.01	
Fe^{3+}	1.00	1.06	1.06
Fe^{2+}			
Mg^{2+}	0.01	0.01	0.01
Mn^{2+}			0.01
Sum B	2.00	2.00	2.00
Si^{4+}	0.04	0.08	0.01
Al^{3+}	0.20	0.30	0.15
Fe^{3+}	0.76	0.59	0.87
Sum T	1.00	0.97	1.03

Footnotes: S.D. = 1σ standard deviation; n—number of analyses; n.d.—not detected.

Table 4. The chemical composition of sharyginite from different localities-literature data.

Sample wt %	[A]	[B]	[C]	[D]	[E]	[F]	[G]	[H]	[I]
	E-2011	M7-184	E-2-1	H-201	YV-411	YV-568	42-17g	M-4	M-4
	Mean	Mean	Mean	Mean	Mean	Mean	Mean	Mean	Mean
	n = 4	n = 19	n = 1	n = 2	n = 1	n = 2	n = 2	n = 1	n = 4
Nb_2O_5	0.17	0.18	0.17	n.d.	n.d.	n.d.	0.06	0.04	0.06
SiO_2	0.53	0.71	0.71	0.60	2.67	0.94	0.62	0.67	0.37
TiO_2	19.55	20.98	18.81	18.59	17.85	17.20	19.66	18.67	20.23
ZrO_2	0.19	0.03	0.12	0.35	n.d.	n.d.	0.45	0.31	0.41
Al_2O_3	4.27	3.21	3.65	4.85	4.65	5.20	5.51	4.30	3.55
Cr_2O_3	0.12	0.01	0.01	0.45	n.d.	n.d.	0.03	0.02	0.06
Fe_2O_3	31.74	30.74	34.34	32.27	30.94	31.13	30.35	33.52	31.95
V_2O_3	n.d.	n.d.	n.d.	n.d.	n.d.	n.d.	n.d.	0.18	0.10
La_2O_3	n.d.	n.d.	n.d.	n.d.	n.d.	n.d.	0.13	n.d.	n.d.
Ce_2O_3	n.d.	n.d.	n.d.	n.d.	n.d.	n.d.	0.17	n.d.	n.d.
CaO	41.12	41.64	41.68	42.48	42.76	42.79	42.73	41.21	41.10
FeO	0.06	0.51	0.03	n.d.	n.d.	n.d.	0.01	n.d.	0.48
MgO	n.d.	0.30	n.d.	0.12	0.45	0.06	0.07	n.d.	n.d.
MnO	0.09	0.38	0.22	0.05	0.54	0.95	n.d.	n.d.	n.d.
SrO	1.78	0.55	0.41	0.20	n.d.	0.15	0.16	1.41	1.29
ZnO	n.d.	n.d.	n.d.	0.07	n.d.	n.d.	n.d.	n.d.	n.d.
Total	99.62	99.24	100.15	100.03	99.86	98.42	99.95	100.33	99.60

Table 4. *Cont.*

Sample	[A]	[B]	[C]	[D]	[E]	[F]	[G]	[H]	[I]
	E-2011	M7-184	E-2-1	H-201	YV-411	YV-568	42-17g	M-4	M-4
Calculated on 8 O									
Ca^{2+}	2.95	2.98	2.97	3.00	3.00	3.08	3.02	2.94	2.96
Sr^{2+}	0.07	0.02	0.02	0.01		0.01	0.01	0.05	0.05
$La^{2+}+Ce^{2+}$							0.01		
Sum A	3.02	3.00	2.99	3.01	3.00	3.09	3.04	2.99	3.01
Nb^{5+}	0.01	0.01	0.01				<0.01	<0.01	<0.01
Ti^{4+}	0.98	1.05	0.94	0.92	0.88	0.87	0.97	0.93	1.02
Zr^{4+}	0.01	<0.01	<0.01	0.01			0.01	0.01	0.01
Cr^{3+}	0.01			0.02			<0.01	<0.01	<0.01
Fe^{3+}	0.98	0.85	1.05	1.02	1.05	1.12	0.97	1.06	0.92
V^{3+}		0.01						0.01	0.01
Fe^{2+}		0.03	<0.01				<0.01		0.03
Mg^{2+}		0.03		0.01	0.04	0.01	0.01		
Mn^{2+}	0.01	0.02	0.01	<0.01	0.03				
Zn^{2+}				<0.01					
Sum B	2.00	2.00	2.01	1.98	2.00	2.00	1.96	2.01	1.99
Si^{4+}	0.04	0.05	0.05	0.04	0.17	0.06	0.04	0.04	0.03
Al^{3+}	0.34	0.25	0.29	0.38	0.36	0.41	0.43	0.34	0.28
Fe^{3+}	0.62	0.69	0.67	0.58	0.47	0.46	0.53	0.62	0.69
Sum T	1.00	0.99	1.01	1.00	1.00	0.93	1.00	1.00	1.00

Footnotes: S.D. = 1σ standard deviation; n—number of analyses; n.d.—not detected; [A–C]—metacarbonate xenoliths in alkali basalt, the Bellerberg volcano, Eastern Eifel, Germany [1,12]; [D]—larnite-ye'elimite rocks from the Hatrurim Basin, Israel [1,3]; [E–F]—larnite bearing rocks from the Hatrurim Basin, Israel [40]; [G]—metacarbonate rocks in the contact with parabasalt, burned dump of mine 42, Kopeisk, Chelyabinsk coal basin, Russia [1,11]; [H–I]—metacarbonate rocks, burned dump of the Kalinin mine, Donetsk coal basin, Ukraine [1,10].

The empirical formula of the holotype sharyginite calculated on the basis of 8 O apfu was $Ca_{3.00}(Fe^{3+}_{1.00}Ti^{4+}_{0.86}Mn^{4+}_{0.11}Zr_{0.01}Cr^{3+}_{0.01}Mg_{0.01})_{\Sigma 2.00}(Fe^{3+}_{0.76}Al_{0.20}Si_{0.04})_{\Sigma 1.00}O_8$, which may be simplified to $Ca_3(Fe^{3+}Ti)\ Fe^{3+}O_8$, as a reflecting end-member formula: $Ca_3(TiFe)FeO_8$ or $Ca_3TiFe_2O_8$. The holotype sharyginite is represented by a complex solid-solution, which contains the following end members: 64% of sharyginite, 20% of shulamitite and 11% of Mn-analogue of sharyginite. Other components like $Ca_3(Zr^{4+}Fe^{3+})Fe^{3+}O_8$, $Ca_3(Fe^{3+}Fe^{3+})Si^{4+}O_8$, $Ca_3(Cr^{3+}Fe^{3+})Si^{4+}O_8$ and $Ca_3(Mg^{2+}Ti^{4+})Si^{4+}O_8$, were minor and their contents were less than 1–2%. The chemical composition of sharyginite from Bellerberg metacarbonate xenoliths was also measured by Sharygin and Wirth [1,12]. The measurements were made for three different samples: E-2011, M7-184, and E-2-1, which are presented in Table 4 as A, B and C, respectively. The differences between these data and the holotype sharyginite were observed in Ti content, which varied between 0.9–1.1 apfu in Sharygin's analyses. In the holotype specimen, lower Ti content was related to Mn^{4+} substitution. Moreover, the iron content in the tetrahedral site indicated that the holotype sharyginite was more enriched in Fe^{3+}. Sharygin also reported small concentrations of Nb^{5+} and Sr^{2+} in his samples [12].

Sharyginite from Jabel Harmun was presented by a solid-solution with prevalent sharyginite $Ca_3TiFeFeO_8$ (62%) and subordinate $Ca_3TiFeAlO_8$ (30%) and $Ca_3Fe(Fe,Cr)SiO_8$ (8%) end members. The mean formula (average of 19 analysis) was $(Ca_{3.03}Sr_{0.01})_{\Sigma 3.04}(Fe^{3+}_{1.06}Ti^{4+}_{0.91}Zr_{0.01}Cr^{3+}_{0.01}Mg_{0.01})_{\Sigma 2.00}(Fe^{3+}_{0.59}Al_{0.30}Si_{0.08})_{\Sigma 0.97}O_8$. Vapnik et al. [40] described opaque minerals occurring within larnite-bearing rocks from the Hatrurm Basin and published some chemical analyses of sharyginite, which were also included in Table 4 (E–F). Sharyginite from these rocks had a similar Ti content as in the holotype sample from the Bellerberg, but relatively lower in comparison with sharyginite from Jabel Harmun. The increase in silicon content (~0.2 apfu) indicated that the iron content in the tetrahedral position does not exceed 0.5 apfu. Despite this, sharyginite end-member prevailed over shulamitite end-member. For example sample YV-411 (E in Table 4) consisted of following end-members: 47% sharyginite, 36% shulamitite, 12% $Ca_3(Cr^{3+}Fe^{3+})Si^{4+}O_8$ and 5% $Ca_3(Mg^{2+}Ti^{4+})Si^{4+}O_8$. Furthermore, chemical analysis for sharyginite from Hatrurim Basin were performed and calculated by Sharygin et al. (D in Table 4) [1,3]. They are very similar in comparison to analysis from Jabel Harmun, mostly in Fe^{3+} and Ti contents, but contained less SiO_2 in chemical composition.

The chemical composition of sharyginite from the Upper Chegem Volcanic Caldera corresponded to the ideal composition. It contained ≈ 85% of sharyginite, 14% of shulamitite, and 1% of Sn or Zr-bearing end members. The empirical formula yielded on four analysis was as follows: $Ca_{3.00}(Fe^{3+}_{1.06}Ti^{4+}_{0.90}Sn^{4+}_{0.01}Zr_{0.01}Mn^{2+}_{0.01}Mg_{0.01})_{\Sigma 2.00}(Fe^{3+}_{0.87}Al_{0.15}Si_{0.01})_{\Sigma 1.03}O_8$.

In literature, there are also chemical data of sharyginite from other metacarbonate rocks, collected on a burned dump of mines in Ukraine [10] and Russia [11]. Sharyginite from Chelyabinsk (G in Table 4) and Donetsk (H-I in Table 4) exhibited similar content of main elements: Fe_2O_3, CaO, TiO_2 and Al_2O_3, like in other localities. Differences were observed in impurities. Sharyginite from Chelyabinsk burned dump contained rare earth elements (REE) such as La and Ce, which were below the detection limit for other mentioned localities. We could observe that samples from Donetsk showed similarities to the Bellerberg samples and in turn, samples from Chelyabinsk were more similar to these from Israel, mainly in the context of tetrahedral position occupation by Al^{3+} and Fe^{3+}.

4.2. X-ray Crystallography

The measured powder data, as well as a calculated pattern, are reported in Table 5. The calculated pattern is based on the structure model obtained from single-crystal data and is generated using *XPow* [41]. Powder data were refined with the Rietveld method using the semi-automatic module in HighScore+ software [42]. Unit-cell parameters refined from the powder data are as follows: $a = 5.4262(4)$ Å, $b = 11.1468(7)$ Å, $c = 5.5308(3)$ Å, $V = 334.5(3)$ Å^3, $Z = 2$.

Table 5. Measured and calculated X-ray powder diffraction data (d in Å) for sharyginite. The strongest diffraction lines are given in bold.

| | | | | Powder Data | | Calculated from the Results of Single-crystal Structure Refinement | |
| | | | | | | | |
h	k	l	I	$d_{meas.}$	$d_{calc.}$	I	d
0	1	0	9	11.0909	11.1641	7	11.1500
0	2	0	5	5.5991	5.5820	4	5.5750
0	1	1	3	4.9385	4.9544	3	4.9527
0	2	1	3	3.9160	3.9281	3	3.9254
1	0	1	8	3.8701	3.8716	11	3.8712
0	3	0	5	3.7127	3.7214	5	3.7167
1	2	1	4	3.1836	3.1813	4	3.1798
0	3	1	6	3.0783	3.0871	5	3.0844
0	0	2	32	2.7633	2.7643	28	2.7640
2	0	0	27	2.7119	2.7118	36	2.7115
1	3	1	100	2.6791	2.6830	100	2.6811
0	4	1	7	2.4874	2.4915	6	2.4890
1	0	2	4	2.4578	2.4628	4	2.4626
1	4	1	7	2.2612	2.2641	6	2.2621
0	3	2	3	-	2.2191	2	2.2179
2	3	0	3	2.1868	2.1916	3	2.1905
2	3	1	2	2.0386	2.0374	2	2.0365
2	0	2	36	1.9359	1.9358	41	1.9356
1	5	1	4	-	1.9342	4	1.9323
2	1	2	3	1.9080	1.9074	3	1.9071
0	6	0	19	1.8566	1.8607	18	1.8583
1	4	2	2	1.8511	1.8467	2	1.8455
2	2	2	3	1.8286	1.8290	3	1.8285
0	2	3	3	1.7554	1.7500	2	1.7496
1	6	1	2	1.6859	1.6771	2	1.6753
0	3	3	4	1.6507	1.6515	4	1.6509
3	2	1	2	1.6393	1.6423	3	1.6419
1	3	3	18	1.5800	1.5798	17	1.5793
3	3	1	12	1.5592	1.5600	16	1.5596
0	6	2	8	1.5450	1.5436	8	1.5422
2	6	0	8	-	1.5342	9	1.5329
3	4	1	2	-	1.4632	2	1.4626
2	3	3	3	1.4064	1.4105	3	1.4101
0	0	4	3	-	1.3821	3	1.3820
4	0	0	3	1.3559	1.3559	4	1.3557
2	6	2	11	1.3410	1.3415	13	1.3405
3	3	3	4	1.2193	1.2193	5	1.2190
4	0	2	2	1.2176	1.2173	2	1.2172
1	9	1	3	1.1806	1.1813	4	1.1799

4.3. Crystal Structure

The crystal structure was refined with Jana2006 [43], starting from the structural model of the synthetic compound $Ca_3TiFe_2O_8$ reported by Rodriguez-Carvajal et al. [6]. As EPMA (electron probe microanalysis) data indicated the presence of up to 3% of Al_2O_3, aluminium was introduced as an additional species on the octahedral as well as on the tetrahedral position. Half of the octahedral site had to be occupied by titanium. Neutral scattering factors and anisotropic displacement parameters were utilized. Furthermore, inversion twinning and isotropic extinction were taken into account. Results showed that an equal amount of twins were present (0.51(3):0.49(3)). Some other crystals showed another type of twinning; a pseudo four-fold axis along b. This was evident in the violation of the $h \neq 2n$ extinction condition of the a-glide plane. The reciprocal space layer *hk0* showed weak reflections at positions h = 1, 3, 5. However, these reflections are slightly displaced with respect to

a*. Furthermore, reflections with *h* = 4 and *h* = 6, showed splitting along a*. This was caused by the 90°-rotation twinning along b, as this superimposed the *0kl* layer onto the layer *hk0*. Figure 7 shows a part of the reconstructed *hk0* layer of a crystal affected by this type of twinning. The reflections belonging to the 90° rotation twin are marked with arrows. With increasing index *h*, their distance from integer *h* positions increased.
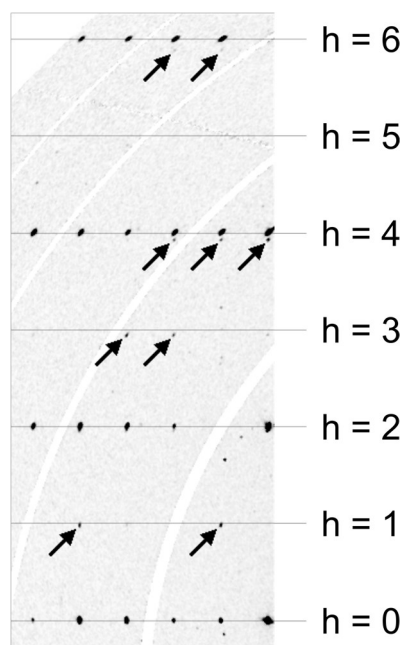
Figure 7. Reconstruction of the reciprocal space layer *hk0* of a crystal affected by 90° rotation twinning. Arrows point to reflections belonging to the smaller twin individual. Synchrotron diffraction data. The curved white bands are caused by gaps between the elements of the Pilatus 2M-F detector and contain no measured data.

The final stage of the refinement included 74 parameters. According to the refinement, the octahedral site is occupied by 3.5% Al, the tetrahedral site exhibits 25% of Al. This corresponds to a composition of x = 0.32 (in $Ca_3TiFe_{2-x}Al_xO_8$). In four additional refinements (using data from further crystals), x was found to vary between 0.26 and 0.38.

Finally, atoms were renumbered, and a cell transformation and origin shift were applied to closely match the model reported for shulamitite [1].

Atom coordinates (x,y,z), occupancies, and equivalent isotropic displacement parameters (U_{iso}, Å^2) for sharyginite are given in Table 6. Anisotropic displacement parameters (Å^2) were summarized in Table 7. The main interatomic distances (Å) are reported in Table 8.

Table 6. Atom coordinates (x,y,z), occupancies and equivalent isotropic displacement parameters (U_{iso}, Å^2) for sharyginite.

Site	Atom	x	y	z	U_{iso}	Occupancy
Ti1	Ti	0.25010(10)	0.16862(4)	0.23966(9)	0.00672(15)	0.5
Fe1	Fe	0.25010(10)	0.16862(4)	0.23966(9)	0.00672(15)	0.465(5)
Al1	Al	0.25010(10)	0.16862(4)	0.23966(9)	0.00672(15)	0.035(5)
Fe2	Fe	0.19825(16)	0.5	0.18318(13)	0.00750(19)	0.751(7)
Al2	Al	0.19825(16)	0.5	0.18318(13)	0.00750(19)	0.249(7)
Ca1	Ca	−0.26824(16)	0.31319(6)	0.27602(11)	0.01048(18)	1
Ca2	Ca	0.2676(3)	0	−0.26624(16)	0.0141(3)	1
O1	O	0.2758(5)	0.35744(18)	0.3210(3)	0.0136(6)	1
O2	O	0.3553(6)	0.5	−0.1222(5)	0.0127(8)	1
O3	O	0.0161(4)	0.15042(14)	0.5135(5)	0.0105(5)	1
O4	O	0.2444(6)	0	0.1700(5)	0.0132(8)	1
O5	O	−0.0146(5)	0.20160(16)	0.0157(5)	0.0127(6)	1

Table 7. Anisotropic displacement parameters (Å^2) for sharyginite.

| Site	Atom	U^{11}	U^{22}	U^{33}	U^{23}	U^{13}	U^{12}
Ti1	Ti	0.0055(3)	0.0109(2)	0.0038(3)	−0.0001(3)	−0.00028(18)	0.00037(14)
Fe1	Fe	0.0055(3)	0.0109(2)	0.0038(3)	−0.0001(3)	−0.00028(18)	0.00037(14)
Al1	Al	0.0055(3)	0.0109(2)	0.0038(3)	−0.0001(3)	−0.00028(18)	0.00037(14)
Fe2	Fe	0.0071(4)	0.0094(3)	0.0060(4)	0	0.0003(3)	0
Al2	Al	0.0071(4)	0.0094(3)	0.0060(4)	0	0.0003(3)	0
Ca1	Ca	0.0131(4)	0.0115(3)	0.0069(3)	−0.0012(4)	0.0015(3)	−0.00057(18)
Ca2	Ca	0.0166(6)	0.0142(4)	0.0116(4)	0	−0.0004(4)	0
O1	O	0.0176(12)	0.0131(9)	0.0099(9)	0.0016(8)	−0.0004(9)	0.0011(7)
O2	O	0.0128(15)	0.0130(13)	0.0124(14)	0	0.0032(13)	0
O3	O	0.0105(9)	0.0129(7)	0.0080(9)	0.0001(8)	0.0014(8)	−0.0008(8)
O4	O	0.0159(17)	0.0122(12)	0.0115(13)	0	−0.0009(13)	0
O5	O	0.0134(11)	0.0177(8)	0.0071(9)	0.0007(8)	−0.0022(8)	−0.0005(9)

The crystal structure of synthetic sharyginite, $Ca_3TiFe_2O_8$, has been described before [6]. It is closely related to the structure of shulamitite [1] and consists of double layers of corner-sharing $(Ti, Fe^{3+})O_6$ octahedra which are separated by single layers of $(Fe^{3+}O_4)$ tetrahedra, which form zweier single-chains (Figure 8). These chains are characteristic for sharyginite, shulamitite and the structurally related brownmillerite.

The sharyginite structure exhibited one octahedrally coordinated site, which hosted titanium and iron, as well as minor amounts of aluminium. The occupation factor of titanium was 0.5, whichwas imposed by the stoichiometry. The tetrahedral site was occupied by iron ($\frac{3}{4}$) and aluminium ($\frac{1}{4}$).

The independent calcium cations were located between the two octahedral layers (Ca2) and between octahedral and tetrahedral layers (Ca1).

**Table 8.** Selected interatomic distances (Å) for sharyginite.

Atom	Atom	distance (Å)
Ti1	O1	2.157(4)
	O3	1.985(4)
	O3	1.996(3)
	O4	1.919(3)
	O5	1.931(3)
	O5	1.938(3)
Mean		1.988
Fe2	O1 × 2	1.812(3)
	O2	1.891(3)
	O2	1.890(3)
Mean		1.851
Ca2	O3 × 2	2.481(3)
	O3 × 2	2.549(3)
	O4	2.887(4)
	O4	2.640(4)
	O4	2.415(3)
	O5 × 2	2.892(3)
Mean		2.643
Ca1	O1	2.534(3)
	O1	2.294(3)
	O2	2.347(3)
	O3	2.719(3)
	O3	2.453(3)
	O5	2.348(3)
	O5	2.436(3)
Mean		2.448
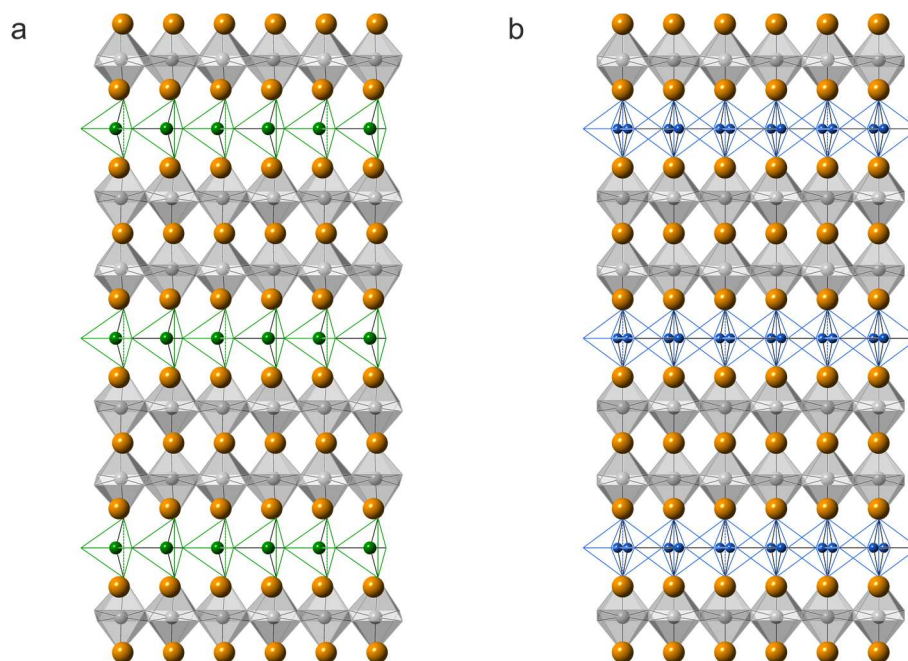
Figure 8. Projections along (001) of the crystal structures of sharyginite (**a**) and shulamitite (**b**). Calcium atoms are shown as orange spheres, $0.5Fe^{3+}/0.5TiO_6$ octahedra are in grey, green, and blue spheres, and bonds corresponding to the tetrahedra centred mainly by Fe^{3+} and Al^{3+} ions, respectively. In shulamitite (**b**), the tetrahedral chains are disordered and both possible configurations are show simultaneously.

4.4. Raman Spectroscopy

In the Raman spectrum of the holotype sharyginite the following main bands were noted (cm^{-1}) (Figure 9a): 114, 145, 190, 248, 307, 389, 486, 560, 710, 752, 785 and 1415, 1475 (overtone). Bands in the OH region were not observed. The spectrum of sharyginite was dominated by an intense Raman band at 710 cm^{-1} which was attributed to ν_1 ($Fe^{3+}O_4$) tetrahedra symmetric stretching vibrations. Two shoulders observed on this band with relative lower intensity at 752 and 785 cm^{-1} were associated with ν_1 (AlO_4) and ν_3 ($Fe^{3+}O_4$) modes, respectively. Bands at 486 and 560 cm^{-1} were related to tetrahedral bending vibrations of ($Fe^{3+}O_4$) group. The low wavenumber region below 400 cm^{-1} was ascribed to the polyhedral CaO_8 and octahedral (Fe^{3+}, Ti)O_6 vibrations [1]. Raman spectra of sharyginite from the other two localities (Figure 9b,c) were similar to the sharyginite spectrum from the Bellerberg. The Raman spectrum was also similar to that of shulamitite [1], with the main distinction in the position of the main band.
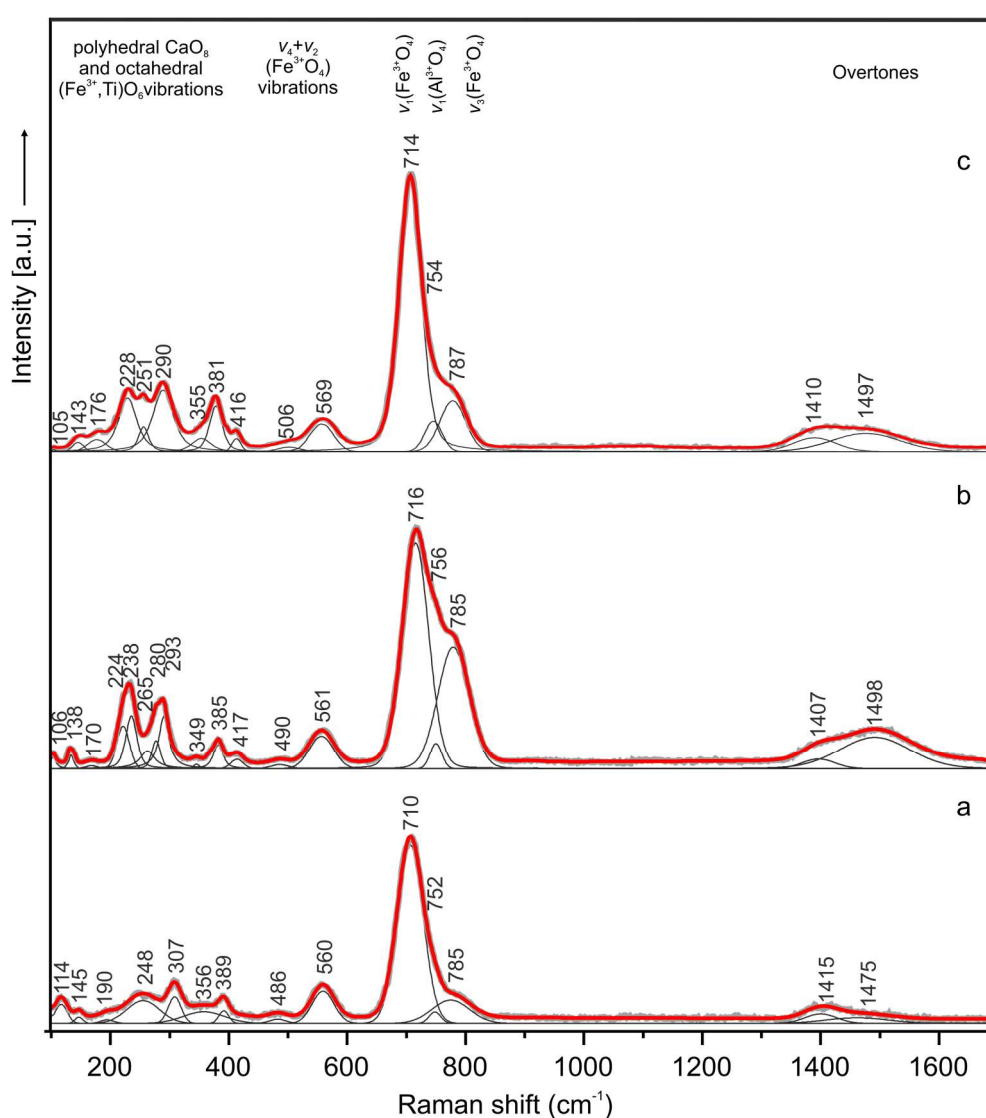
Figure 9. Raman spectra of sharyginite from the Bellerberg volcano (**a**), Jabel Harmun (**b**) and Upper Chegem Volcanic Caldera (**c**) localities.

5. Discussion

The difference between sharyginite, $Ca_3TiFe_2O_8$ and shulamitite, $Ca_3TiFeAlO_8$, is related to the occupancy of the tetrahedral site by Fe^{3+} and Al, respectively and the space group symmetry. The holotype sharyginite from the Bellerberg volcano is close to $Ca_3TiFe(Fe_{0.8}Al_{0.2})O_8$, whereas sharyginite compositions from the Upper Chegem Caldera and the Hatrurim Complex show greater diversity (Tables 3 and 4). The iron content in the holotype specimen, obtained from the refinement calculation, may be slightly overestimated, due to the Mn^{4+} substitution (up to 2.3%, Table 3). Comparing results of chemical composition from the different localities and other authors data we also note the presence of insignificant impurities such as Zr, Sr, Nb, Sn, Mn and REE. The wide variation of trivalent iron and aluminium in the chemical composition allows us to claim that a continuous solid solution exists between sharyginite and shulamitite. This solid solution may be compared with the brownmillerite, $Ca_2(Fe^{3+},Al)O_5$—srebrodolskite, $Ca_2Fe^{3+}_2O_5$ series. All mentioned minerals belong to anion-deficient, perovskites and show differences in TO_4 tetrahedra orientation between end-members which are related to the adopted space group [2].

At a first glance, the main structural differences between shulamitite and sharyginite appear to be in tetrahedral layers: shulamitite exhibits disorder of two possible configurations of the tetrahedral chain, whereas in sharyginite, only one type of chain exists, which also results in the structure being acentric. Looking more closely, another striking difference can be noted in the octahedral layers: Figure 10 shows a view perpendicular to the octahedral layers of both structures. In shulamitite (*Pmma*), the oxygen atoms O3 and O5 reside on the two-fold axis 2[010]. As a consequence, the octahedra cannot be rotated around the b-axis, as their O3-O5 edges are constrained to be parallel to a and c (Figure 10a). The lower symmetry in sharyginite (*P2$_1$ma*) does not restrict O3 and O5 on a special position, thus allowing the octahedra to rotate around b. The rotation, which can be seen in Figure 10b, is 3.15°. The reason for this rotation is most likely an adaption to the configuration of the tetrahedral chains. As discussed earlier [44], the tetrahedral chains exhibit a dipole moment. In shulamitite, all chains are disordered, resulting in a net dipole moment of zero. Only one type of chain occurs in sharyginite, therefore dipole moments have to be compensated by distortions of the octahedral layers and displacement of Ca cations.

The occurrence of a morphotropic phase boundary (depending on the Al-content) between sharyginite and shulamitite is comparable to the one between srebrodolskite and brownmillerite [45] and will be the subject of another study.
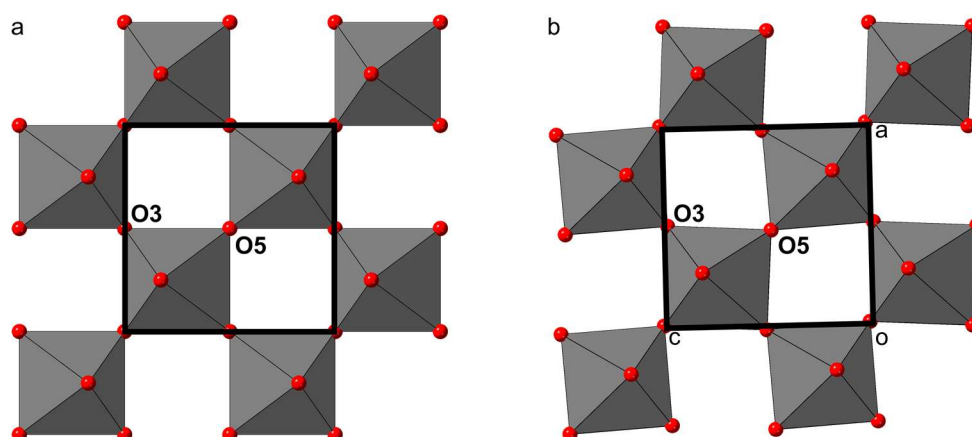
Figure 10. The arrangement of the octahedral layers in shulamitite (**a**) and sharyginite (**b**). Rotation of the octahedra is restricted by symmetry in shulamitite, as O3 and O5 reside on special positions. The lower symmetry of sharyginite allows the octahedra to rotate.

In metacarbonate xenoliths from the Bellerberg locality, the occurrence of sharyginite in association with perovskite is common. The phase relationship indicates that sharyginite is a later phase and overgrows the perovskite or even replaces it, which is very well presented in Figure 4. We suggest that new mineral sharyginite is formed at high-temperature conditions. According to the $CaTiO_3$-$Ca_2Fe_2O_5$ diagram [46], the stoichiometric $Ca_3TiFe_2O_8$ phase and disordered cubic Fe-perovskite are stable at temperatures above 1160°C. Under this temperature in the composition field $0.5 < x < 0.67$, $Ca_3TiFe_2O_8$ coexists with $Ca_4Ti_2Fe_2O_{11}$ phase. In turn in $0.67 < x < 1.00$, two ordered phases: $Ca_3TiFe_2O_8$ and $Ca_2Fe_2O_5$ coexist under 1400°C [3,46]. Moreover, for some larnite rocks of the Hatrurim Complex, where sharyginite was also identified, the minimum temperature of formation was estimated from Fe-perovskite-$Ca_3TiFe_2O_8$ mineral paragenesis. This temperature is in the range of 1170–1200°C [3]. Synthetic data also indicate the formation of $Ca_3TiFe_2O_8$ phase at high temperature (>1000°C) [4,6]. Furthermore, the coexistence of Fe-perovskite and $Ca_3TiFe_2O_8$ phases (sharyginite) may be used for the temperature evaluation of mineral associations in pyrometamorphic systems. However, it is necessary to take into account the specific composition of Fe-perovskite and the modal phase relationship in the association and to be sure that the phases were crystallized under conditions close to equilibrium [10].

References

1. Sharygin, V.V.; Lazic, B.; Armbruster, T.M.; Murashko, M.N.; Wirth, R.; Galuskina, I.O.; Galuskin, E.V.; Vapnik, Y.; Britvin, S.N.; Logvinova, A.M. Shulamitite $Ca_3TiFe^{3+}AlO_8$—A new perovskite-related mineral from Hatrurim Basin, Israel. *Eur. J. Miner.* **2013**, *25*, 97–111. [CrossRef]

2. Mitchell, R.H.; Welch, M.D.; Chakhmouradian, A.R.; Mills, S. Nomenclature of the perovskite supergroup: A hierarchical system of classification based on crystal structure and composition. *Miner. Mag.* **2017**, *81*, 411–461. [CrossRef]

3. Sharygin, V.V.; Sokol, E.V.; Vapnik, Y. Minerals of the pseudobinary perovskite-brownmillerite series from combustion metamorphic larnite rocks of the Hatrurim Formation (Israel). *Russ. Geol. Geophys.* **2008**, *49*, 709–726. [CrossRef]

4. Grenier, J.-C.; Darriet, J.; Pouchard, M.; Hagenmuller, P. Mise en evidence d'une nouvelle famille de phases de type perovskite lacunaire ordonnee de formule $A_3M_3O_8$ ($AMO_{2,67}$). *Mater. Res. Bull.* **1976**, *11*, 1219–1225. [CrossRef]

5. Grenier, J.-C.; Pouchard, M.; Hagenmuller, P. Vacancy ordering in oxygen-deficient perovskite-related ferrites. In *Ferrites Transitions Elements Luminescence. Structure and Bonding*; Springer-Verlag: Berlin, Germany, 1981; Volume 47, pp. 1–25.

6. Rodríguez-Carvajal, J.; Vallet-Regí, M.; Calbet, J.M.G. Perovskite threefold superlattices: A structure determination of the $A_3M_3O_8$ phase. *Mater. Res. Bull.* **1989**, *24*, 423–430. [CrossRef]

7. Causa, M.T.; Zysler, R.D.; Tovar, M.; Vallet-Regí, M.; González-Calbet, J.M. Magnetic properties of the $Ca_nFe_2Ti_{n-2}O_{3n-1}$ perovskite related series: An EPR study. *J. Solid State Chem.* **1992**, *98*, 25–32. [CrossRef]

8.   Galuskin, E.V.; Gazeev, V.M.; Armbruster, T.; Zadov, A.E.; Galuskina, I.O.; Pertsev, N.N.; Dzierżanowski, P.; Kadiyski, M.; Gurbanov, A.G.; Wrzalik, R.; et al. Lakargiite CaZrO$_3$: A new mineral of the perovskite group from the North Caucasus, Kabardino-Balkaria, Russia. *Am. Miner.* **2008**, *93*, 1903–1910. [CrossRef]

9.   Niedermayr, G.; Auer, C.; Bernhard, F.; Brandstätter, F.; Gröbner, J.; Hammer, V.M.F.; Knobloch, G.; Koch, G.; Kolitchs, U.; Konzett, J.; et al. Neue Mineralfunde aus Österreich LX. *Carinth. II* **2011**, *201*, 135–186.

10.   Sharygin, V.V. *Lakargiite and Minerals of the Perovskite Brownmillerite Series in Metacarbonate Rocks from Donetsk Burned Dumps*; Scientific works of Donetsk National Technical University, Mining and Geological Series; Donetsk National Technical University: Donetsk, Ukraine, 2011; Volume 15, pp. 114–125.

11.   Sharygin, V.V. Minerals of the Ca$_3$TiFeAlO$_8$–Ca$_3$TiFeFeO$_8$ series in natural and technogenic pyrometamorphic systems. In *The Mineralogy of Technogenesis 2012*; Institute of Mineralogy, Uralian Branch of Russian Academy of Sciences: Miass, Russia, 2012; pp. 29–49.

12.   Sharygin, V.V.; Wirth, R. Shulamitite and its Fe-analog in metacarbonate xenoliths from alkali basalts, E. Eifel, Germany. In Proceedings of the 29th International Conference Ore Potential of Alkaline, Kimberlite and Carbonatite Magmatism, "Alkaline magmatism of the Earth", Sudak-Moscow, Ukraine-Russia, 14–22 September 2012.

13.   Mihajlović, T.; Lengauer, C.L.; Ntaflos, T.; Kolitsch, U.; Tillmanns, E. Two new minerals rondorfite, Ca$_8$Mg[SiO$_4$]$_4$Cl$_2$, and almarudite, K.($\square$,Na)$_2$(Mn,Fe,Mg)$_2$(Be,Al)$_3$[Si$_{12}$O$_{30}$], and a study of iron-rich wadalite, Ca$_{12}$[(Al$_8$Si$_4$Fe$_2$)O$_{32}$]Cl$_6$, from the Bellerberg (Bellberg) volcano, Eifel, Germany. *Neues Jahrb. Miner.* **2004**, *179*, 265–294. [CrossRef]

14.   Hentschel, G. *Die Mineralien der Eifelvulkane*, 2nd ed.; Weise Verlag: München, Germany, 1987.

15.   Abraham, K.; Gebert, W.; Medenbach, O.; Schreyer, W.; Hentschel, G. Eifelite, KNa$_3$Mg$_4$Si$_{12}$O$_{30}$, a new mineral of the osumilite group with octahedral sodium. *Contrib. Miner. Pet.* **1983**, *82*, 252–258. [CrossRef]

16.   Irran, E.; Tillmanns, E.; Hentschel, G. Ternesite, Ca$_5$(SiO$_4$)$_2$(SO$_4$), a new mineral from the Ettringer Bellerberg/Eifel, Germany. *Miner. Petrol.* **1997**, *60*, 121–132. [CrossRef]

17.   Galuskin, E.V.; Krüger, B.; Krüger, H.; Blass, G.; Widmer, R.; Galuskina, I.O. Wernerkrauseite, CaFe^{3+}$_2$Mn^{4+}O$_6$: The first nonstoichiometric post-spinel mineral, from Bellerberg volcano, Eifel, Germany. *Eur. J. Miner.* **2016**, *28*, 485–493. [CrossRef]

18.   Gazeev, V.M.; Zadov, A.E.; Gurbanov, A.G.; Pertsev, N.N.; Mokhov, A.V.; Dokuchaev, A.Y. Rare minerals from Verkhniechegemskaya caldera (in xenoliths of skarned limestone). *Vestnik. Vladikavkazskogo Nauchnogo Centra.* **2006**, *6*, 18–27.

19.   Grapes, R. *Pyrometamorphism*, 2nd ed.; Springer-Verlag: Berlin Heidelberg, Germany, 2010.

20.   Galuskin, E.V.; Gazeev, V.M.; Lazic, B.; Armbruster, T.; Galuskina, I.O.; Zadov, A.E.; Pertsev, N.N.; Wrzalik, R.; Dzierżanowski, P.; Gurbanov, A.G.; et al. Chegemite Ca$_7$(SiO$_4$)$_3$(OH)$_2$—A new humite-group calcium mineral from the Northern Caucasus, Kabardino-Balkaria, Russia. *Eur. J. Miner.* **2009**, *21*, 1045–1059. [CrossRef]

21.   Galuskina, I.O.; Galuskin, E.V.; Armbruster, T.; Lazic, B.; Kusz, J.; Dzierżanowski, P.; Gazeev, V.M.; Pertsev, N.N.; Prusik, K.; Zadov, A.E.; et al. Elbrusite-(Zr)—A new uranian garnet from the Upper Chegem caldera, Kabardino-Balkaria, Northern Caucasus, Russia. *Am. Miner.* **2010**, *95*, 1172–1181. [CrossRef]

22.   Galuskin, E.V.; Galuskina, I.O.; Lazic, B.; Armbruster, T.; Zadov, A.E.; Krzykawski, T.; Banasik, K.; Gazeev, V.M.; Pertsev, N.N. Rusinovite, Ca$_{10}$(Si$_2$O$_7$)$_3$Cl$_2$: A new skarn mineral from the Upper Chegem caldera, Kabardino-Balkaria, Northern Caucasus, Russia. *Eur. J. Miner.* **2011**, 837–844. [CrossRef]

23.   Galuskin, E.V.; Gfeller, F.; Savelyeva, V.B.; Armbruster, T.; Lazic, B.; Galuskina, I.O.; Többens, D.M.; Zadov, A.E.; Dzierżanowski, P.; Pertsev, N.N.; et al. Pavlovskyite Ca$_8$(SiO$_4$)$_2$(Si$_3$O$_{10}$): A new mineral of altered silicate-carbonate xenoliths from the two Russian type localities, Birkhin massif, Baikal Lake area and Upper Chegem caldera, North Caucasus. *Am. Miner.* **2012**, *97*, 503–512. [CrossRef]

24.   Galuskin, E.V.; Lazic, B.; Armbruster, T.; Galuskina, I.O.; Pertsev, N.N.; Gazeev, V.M.; Włodyka, R.; Dulski, M.; Dzierżanowski, P.; Zadov, A.E.; et al. Edgrewite Ca$_9$(SiO$_4$)$_4$F$_2$-hydroxyledgrewite Ca$_9$(SiO$_4$)$_4$(OH)$_2$, a new series of calcium humite-group minerals from altered xenoliths in the ignimbrite of Upper Chegem caldera, Northern Caucasus, Kabardino-Balkaria, Russia. *Am. Miner.* **2012**, *97*, 1998–2006. [CrossRef]

25.   Galuskina, I.O.; Galuskin, E.V.; Kusz, J.; Dzierżanowski, P.; Prusik, K.; Gazeev, V.M.; Pertsev, N.N.; Dubrovinsky, L. Dzhuluite, Ca$_3$SbSnFe^{3+}$_3$O$_{12}$, a new bitikleite-group garnet from the Upper Chegem Caldera, Northern Caucasus, Kabardino-Balkaria, Russia. *Eur. J. Miner.* **2013**, 231–239. [CrossRef]

26. Galuskina, I.O.; Krüger, B.; Galuskin, E.V.; Armbruster, T.; Gazeev, V.M.; Włodyka, R.; Dulski, M.; Dzierżanowski, P. Fluorchegemite, $Ca_7(SiO_4)_3F_2$, a new mineral from the edgrewitw-bearing endoskarn zone of an altered xenolith in ignimbrites from Upper Chegem Caldera, Northern Caucasus, Kabardino-Balkaria, Russia: Occurrence, crystal structure, and new data on the mineral assemblages. *Can. Miner.* **2015**, *53*, 325–344.

27. Galuskin, E.V.; Galuskina, I.O.; Kusz, J.; Armbruster, T.; Marzec, K.M.; Dzierżanowski, P.; Murashko, M. Vapnikite Ca_3UO_6—A new double-perovskite mineral from pyrometamorphic larnite rocks of the Jabel Harmun, Palestinian Autonomy, Israel. *Miner. Mag.* **2014**, *78*, 571–581. [CrossRef]

28. Galuskina, I.O.; Vapnik, Y.; Lazic, B.; Armbruster, T.; Murashko, M.; Galuskin, E.V. Harmunite $CaFe_2O_4$: A new mineral from the Jabel Harmun, West Bank, Palestinian Autonomy, Israel. *Am. Miner.* **2014**, *99*, 965–975. [CrossRef]

29. Galuskin, E.V.; Gfeller, F.; Armbruster, T.; Galuskina, I.O.; Vapnik, Y.; Dulski, M.; Murashko, M.; Dzierżanowski, P.; Sharygin, V.V.; Krivovichev, S.V.; et al. Mayenite supergroup, part III: Fluormayenite, $Ca_{12}Al_{14}O_{32}[\square_4F_2]$, and fluorkyuygenite, $Ca_{12}Al_{14}O_{32}[(H_2O)_4F_2]$, two new minerals from pyrometamorphic rocks of the Hatrurim Complex, South Levant. *Eur. J. Miner.* **2015**, *27*, 123–136. [CrossRef]

30. Galuskin, E.V.; Gfeller, F.; Armbruster, T.; Galuskina, I.O.; Vapnik, Y.; Murashko, M.; Włodyka, R.; Dzierżanowski, P. New minerals with a modular structure derived from hatrurite from the pyrometamorphic Hatrurim Complex. Part I. Nabimusaite, $KCa_{12}(SiO_4)_4(SO_4)_2O_2F$, from larnite rocks of Jabel Harmun, Palestinian Autonomy, Israel. *Miner. Mag.* **2015**, *79*, 1061–1072. [CrossRef]

31. Galuskin, E.V.; Gfeller, F.; Galuskina, I.O.; Armbruster, T.; Krzạtała, A.; Vapnik, Y.; Kusz, J.; Dulski, M.; Gardocki, M.; Gurbanov, A.G.; et al. New minerals with a modular structure derived from hatrurite from the pyrometamorphic rocks. Part III. Gazeevite, $BaCa_6(SiO_4)_2(SO_4)_2O$, from Israel and the Palestine Autonomy, South Levant, and from South Ossetia, Greater Caucasus. *Miner. Mag.* **2017**, *81*, 499–513. [CrossRef]

32. Galuskina, I.O.; Galuskin, E.V.; Prusik, K.; Vapnik, Y.; Juroszek, R.; Jeżak, L.; Murashko, M. Dzierżanowskite, $CaCu_2S_2$—A new natural thiocuprate from Jabel Harmun, Judean Desert, Palestine Autonomy, Israel. *Miner. Mag.* **2017**, *81*, 1073–1085. [CrossRef]

33. Gross, S. *The Mineralogy of the Hatrurim Formation Israel*; Geological Survey of Israel: Jerusalem, Israel, 1977.

34. Burg, A.; Starinsky, A.; Bartov, Y.; Kolodny, Y. Geology of the Hatrurim Formation ("Mottled Zone") in the Hatrurim basin. *Isr. J. Earth Sci.* **1991**, *40*, 107–124.

35. Sokol, E.V.; Novikov, I.S.; Vapnik, Y.; Sharygin, V.V. Gas fire from mud volcanoes as a trigger for the appearance of high-temperature pyrometamorphic rocks of the Hatrurim Formation (Dead Sea area). *Dokl. Earth Sci.* **2007**, *413*, 474–480. [CrossRef]

36. Novikov, I.; Vapnik, Y.; Safonova, I. Mud volcano origin of the Mottled Zone, South Levant. *Geosci. Front.* **2013**, *4*, 597–619. [CrossRef]

37. Waltersperger, S.; Olieric, V.; Pradervand, C.; Glettig, W.; Salathe, M.; Fuchs, M.R.; Curtin, A.; Wang, X.; Ebner, S.; Panepucci, E.; et al. PRIGo: A new multi-axis goniometer for macromolecular crystallography. *J. Synchrotron Radiat.* **2015**, *22*, 895–900. [CrossRef] [PubMed]

38. Wojdyla, J.A.; Kaminski, J.W.; Panepucci, E.; Ebner, S.; Wang, X.; Gabadinho, J.; Wang, M. DA+ data acquisition and analysis software at the Swiss Light Source macromolecular crystallography beamlines. *J. Synchrotron Radiat.* **2018**, *25*, 293–303. [CrossRef] [PubMed]

39. Kabsch, W. XDS. *Acta Cryst. D Biol. Cryst.* **2010**, *66*, 125–132. [CrossRef] [PubMed]

40. Vapnik, Y.; Galuskina, I.O.; Palchik, V.; Sokol, E.V.; Galuskin, E.V.; Lindsley-Griffin, N.; Stracher, G. Paralavas in combustion metamorphic complex at the Hatrurim Basin, Israel. In *Coal and Peat Fires: A Global Perspective*, 1st ed.; Elsevier: Amsterdam, Netherlands, 2014; Volume 3, pp. 281–316.

41. Downs, R.T.; Bartelmehs, K.L.; Gibbs, G.V.; Boisen, M.B. Interactive software for calculating and displaying X-ray or neutron powder diffractometer patterns of crystalline materials. *Am. Miner.* **1993**, *78*, 1104–1107.

42. Degen, T.; Sadki, M.; Bron, E.; König, U.; Nénert, G. The HighScore suite. *Powder Diffr.* **2014**, *29*, S13–S18. [CrossRef]

43. Petříček, V.; Dušek, M.; Palatinus, L. Crystallographic Computing System JANA2006: General features. *Z. Kristallogr. Cryst. Mater.* **2014**, *229*, 345–352. [CrossRef]

44. Abakumov, A.M.; Kalyuzhnaya, A.S.; Rozova, M.G.; Antipov, E.V.; Hadermann, J.; Van Tendeloo, G. Compositionally induced phase transition in the $Ca_2MnGa_{1-x}Al_xO_5$ solid solutions: Ordering of tetrahedral chains in brownmillerite structure. *Solid State Sci.* **2005**, *7*, 801–811. [CrossRef]

45. Redhammer, G.J.; Tippelt, G.; Roth, G.; Amthauer, G. Structural variations in the brownmillerite series $Ca_2(Fe_{2-x}Al_x)O_5$: Single-crystal X-ray diffraction at 25 °C and high-temperature X-ray powder diffraction (25 °C $\leq$ T $\leq$ 1000 °C). *Am. Miner.* **2004**, *89*, 405–420. [CrossRef]

46. Becerro, A.; McCammon, C.; Langenhorst, F.; Seifert, F.; Angel, R.J. Oxygen-vacancy ordering in $CaTiO_3$-$CaFeO_{2.5}$ perovskites: From isolated defects to infinite sheets. *Phase Transit.* **1999**, *69*, 133–146. [CrossRef]